Int. J. Electrochem. Sci., 7 **(2012)** 387 - 404

International Journal of
ELECTROCHEMICAL
SCIENCE
www.electrochemsci.org

Label-Free Detection of Creatinine Using a Disposable Poly-N-Isopropylacrylamide as an Encapsulating Creatinine Deiminase Based $Eu_2Ti_2O_7$ Electrolyte-Insulator-Semiconductors

Jim-Long Her[1], *Chao-Wen Lin*[2], *Kung-Yuan Chang*[2], *and Tung-Ming Pan*[2,*]

[1] Division of Natural Science, Center for General Education, Chang Gung University, Taoyuan 333, Taiwan, R. O. C.
[2] Department of Electronics Engineering, Chang Gung University, Taoyuan 333, Taiwan, R. O. C.
[*]E-mail: tmpan@mail.cgu.edu.tw

Received: 11 November 2011 / *Accepted:* 2 December 2011 / *Published:* 1 January 2012

In this study, we propose an electrolyte–insulator–semiconductor (EIS) device fabricating from high-k Eu_2O_3 and $Eu_2Ti_2O_7$ sensing membranes deposited on Si substrates through reactive radio frequency sputtering for biomedical engineering applications. We used x-ray diffraction, x-ray photoelectron spectroscopy, and atomic force microscopy to explore the structural and morphological features of these films with annealing at various temperatures. Compared with Eu_2O_3 film, $Eu_2Ti_2O_7$ electrolyte-insulator-semiconductor devices annealed at 900 °C exhibited a higher sensitivity (59.03 mV/pH in the solutions from pH 2 to 12), a smaller hysteresis voltage (2.8 mV in the pH loop 7→4→7→10→7), and a lower drift rate (0.616 mV/h in the pH 7 buffer solution), presumably because of its higher surface roughness and its thinner low-*k* interfacial layer at the oxide/Si interface. In addition, a disposable poly-*N*-isopropylacrylamide (PNIPAAm) was used as an encapsulating creatinine deiminase, making easily the loading and removal of a biological recognition element on a biosensor. PNIPAAm film has reversible solubility to become a solution-gelatin state change in response to thermal condition (~32 °C). The high-κ $Eu_2Ti_2O_7$ creatinine biosensor annealed at 900 °C allowed the potentiometric analysis of creatinine, at concentrations ranging from 10^{-1} to 10^{-6} M, with a sensitivity of 42.22 mV/$pC_{creatinine}$.

Keywords: electrolyte–insulator–semiconductor (EIS); Eu_2O_3; $Eu_2Ti_2O_7$; creatinine.

1. INTRODUCTION

Many analytical methods can be used for determination of a large number of biochemical analytes. However, they require well-equipped laboratories and professional staff to operate the instruments. A modern analytical tool for biochemical and medical applications should satisfy several

requirements, including minimal volume of the sample and reagent and high selectivity for the analyte. Complementary metal–oxide–semiconductor (CMOS) technology gives an opportunity to achieve these requirements in respect to the sensing and signal processing because of its small size and low cost. Among various types of chemical sensors are the ion–sensitive field–effect–transistors (ISFETs) for detection of biologically relevant ions, such as hydrogen (pH), potassium, sodium, calcium and ammonium [1-2]. The Metal-oxide-semiconductor field-effect-transistor (MOSFET) device consists mainly of the metal, the oxide, the source/drain, and the semiconductor substrate; the difference between a MOSFET and an ISFET device is that no metal gate electrode is used in the later. Caras et al. [3] showed the first use of ISFET for the detection of penicillin; since then, this device has been developed to detect a variety of biomolecules, including urea, lactate, and glucose [1-2, 4]. The sensing mechanism involves immobilized probe molecules (e.g., enzymes) reacting specifically with the target biomolecules, thus causing a change in pH at the enzyme–membrane/electrolyte interface. This local pH change, closely correlating with the concentration of the detected target, is then measured by the ISFET device. Various gate dielectric materials (e.g., Si_3N_4, Al_2O_3, Ta_2O_5, TiO_2) [2, 5-7], have been employed to achieve the pH response. Furthermore, several high-dielectric-constant (high-κ) metal oxide materials (e.g., ZrO_2, HfO_2, Gd_2O_3, Er_2O_3, Yb_2O_3) [8-12] have been employed recently as pH-sensitive membranes in electrolyte–insulator–semiconductor (EIS) devices because of their good sensing performance. To improve the quality of the interface between the high-κ material and the Si substrate, the growth of a thin SiO_2 film on the Si substrate imparts the pH-sensing film with a smaller density of the interfacial state, lower stress, and good adhesion [13].

With their high dielectric constants, high resistivities, and large bandgap energies, rare-earth (RE) thin oxides are promising candidates as replacement materials for conventional SiO_2 films for advanced CMOS devices [14-15]. Among them, Eu_2O_3 film can be considered for high-k gate dielectric applications due to its high dielectric constant, large bandgap, and good thermal stability with Si [15]. Moreover, Paivasaari et al. [16] demonstrated that thin Eu_2O_3 film had a low leakage current of ~10^{-9} A/cm^2. The main concerns of RE films are the moisture absorption, which degrades their permittivity through the formation of low-permittivity hydroxides. To overcome the problem of moisture absorption, the incorporation of Ti or TiO_2 into the RE dielectric films can result in improved physical and electrical properties (a thinner interfacial layer, lower solubility in water, higher capacitance, and lower leakage current) because it decreases the extent of the reaction of the dielectric film with water [17-19].

Methods for enzyme immobilization can be classified into three basic categories: (1) carrier-binding method, (2) cross-linking method, and (3) entrapping method [14]. For carrier-binding method, the enzyme molecules are covalently bound onto the surface of a transducer by using chemical species as a linker.

Nevertheless, this method might have some drawbacks for biosensing applications such as poor reproducibility, lower dynamic range, difficulty in preserving and controlling enzyme activities, and short lifetime [20–21]. The entrapment method of immobilization, in which the enzyme molecules are encapsulated in the 3-dimensional (3-D) network of a polymer film to a transducer, is generally believed to carry out the immobilization reaction under mild conditions to possibly minimize the alteration or loss of enzyme activity.

The gel entrapment method has been widely used for immobilization of an enzyme [22]. However, one technical problem is that the repeated operations of biosensing might cause cross contamination, and thus they lead to detection biases. This could be simply improved by the use of a fresh enzyme/polymer film for each biosensing if this film can become disposable.

Thermosensitive polymer film has attracted more attention among various intelligent hydrogels, because it can possess solution-gelatin transitions by simply manipulating the environmental temperature.

Poly-*N*-isopropylacrylamide (PNIPAAm) film has reversible solubility to obtain a solution-gelatin state change in response to thermal condition. The phase transition temperature of PNIPAAm is around 32 °C. Below the temperature, such a PNIPAAm film exhibits a higher solubility in water, whereas its hydrogen bond interactions are weakened or destroyed as the increasing temperature, resulting in a lower solubility of PNIPAAm in water, and thus becoming in a gel state [23-24]. In this paper, we described the structural and sensing characteristics of Eu_2O_3 and $Eu_2Ti_2O_7$ sensing films deposited on Si substrates by means of reactive radio frequency (rf) sputtering. We applied X-ray diffraction (XRD) to determine the growth directions and crystallinity of the films, X-ray photoelectron spectroscopy (XPS) to analyze the chemical structure of the Eu_2O_3 and $Eu_2Ti_2O_7$ films, and atomic force microscopy (AFM) to monitor the surface morphology of the sensing films after annealing at different temperatures.

We found that the post-deposition annealing (PDA) temperature played an important role in the formation of the low-k interfacial layer at the oxide-Si interface.

Furthermore, we determined the effect of PDA treatment on the sensing characteristics (pH sensitivity, hysteresis, and drift) of the Eu_2O_3 and $Eu_2Ti_2O_7$ films. Finally, we demonstrate that the hybrid configuration of a $Eu_2Ti_2O_7$-based EIS with an attached creatinine deiminase–immobilizing PNIPAAm allows for the detection of creatinine.

2. EXPERIMENTAL

Eu_2O_3 and $Eu_2Ti_2O_7$ EIS devices were fabricated on 4 in. p-type (100) Si wafers having a resistivity of 5–10 Ω-cm. Wafers were cleaned using a standard Radio Corporation of America (RCA) process and then they were dipped in dilute HF for 10 s to remove the native oxide from the surface. After RCA cleaning, an ~20 nm Eu_2O_3 film was deposited on the Si substrate by reactive rf sputtering from an europium oxide target in diluted O_2 ambient (Ar/O_2=5 sccm/2 sccm) at a substrate temperature of 27 °C, whereas an ~20 nm $Eu_2Ti_2O_7$ film was deposited by reactive rf cosputtering from an europium oxide target and titanium target. All samples were subjected to rapid thermal annealing (RTA) in an O_2 ambient for 30 s at temperatures ranging from 700 to 900 °C to form Eu_2O_3 and $Eu_2Ti_2O_7$ structures.

The backside contact (a 400-nm-thick Al film) of the Si wafer was deposited using a thermal coater. The sensing membrane size was defined through photolithographic processing under a photosensitive epoxy (SU8-2005, MicroChem Inc.) that behaves as an antiacid polymer.

EIS devices were then fabricated on the copper lines of a printed circuit board by using a silver gel to form conductive lines. A hand-made epoxy package was used to encapsulate the EIS structure and the copper line.

The film structures of the Eu_2O_3 and $Eu_2Ti_2O_7$ sensing films after RTA at different temperatures were studied by XRD. XRD analyses were carried out using a Siemens D5000 with a Cu K_α (λ = 1.542 Å) radiation. The composition and chemical bonding in Eu_2O_3 and $Eu_2Ti_2O_7$ films were investigated using a Physical Electronics Quantum 2000 XPS instrument. The surface morphologies of the films were observed using an NT-MDT Solver P47 (AFM). The AFM was operated in the tapping mode for imaging; the scan area for measurement of the roughness was 1x1 μm. The pH sensitivities of the Eu_2O_3 and $Eu_2Ti_2O_7$ sensing membranes were determined by measuring capacitance–voltage (C–V) curves of the EIS devices. The C–V curves were measured using buffer solutions of various values of pH (Merck Inc.), a Ag/AgCl reference electrode, and a Hewlett–Packard 4284A LCR meter operated at an ac signal frequency of 100 Hz. All setups were performed in a dark box to avoid interference from light and noise.

In preparation, 1.0 g PNIPAAm (99 %, Acros Organics, Taiwan) was thoroughly dissolved in 20 ml distilled water at 60 °C using a hot water bath, and followed by cooling to a room temperature (25 °C). 200 μl ammonium peroxodisulfate (APS, 98.7% pure; unless otherwise stated all chemicals were purchased from Sigma, Taiwan), and 50 μl N,N,N,N-Tetramethylethylenediamine (TEMED, 99% pure) were then added to the prepared PNIPAAm suspension, and kept at a room temperature for 30 h to allow polymerization. The PNIPAAm suspension was then mixed thoroughly with a creatinine deiminase (from Jack Beans, ~36 U/mg) solution prepared in phosphate buffered saline (PBS) to form a creatinine deiminase/PNIPAAm suspension with the PNIPAAm and creatinine deiminase concentrations of 0.44 M and 0.1 mg/L, respectively.

For creatinine biosensing operations, the $Eu_2Ti_2O_7$ EIS sensor was first placed on the surface of a transparent indium tin oxide (ITO)-based microheater chip to provide a tunable thermal condition. The temperature was set at 37 °C first, and succeeded by loading the 80 μl creatinine deiminase/PNIPAAm suspension onto the defined sensing zone.

The loaded gel suspension was spread horizontally using a glass slide, by which the volume of the cavity above the sensing zone quantitatively defines the loaded volume of creatinine deiminase/PNIPAAm suspension. After the gelation of such suspension was completed (~5-10 s), the head of the assembled device was immersed into the creatinine standard solutions with different concentrations. The pH levels of each creatinine solutions were checked by a commercial pH meter to guarantee the background pH level is equal. 1-min measurement time was set to equilibrate each tested condition, and followed by recording the *C-V* relationship.

After experiments, the creatinine deiminase/PNIPAAm gel film on the surface of a $Eu_2Ti_2O_7$ EIS sensor was then completely removed simply by decreasing its temperature. The re-solubilized polymer suspension was then washed away using R.O. water afterwards.

By this design, the biological recognition element on a biosensor device can easily become disposable.

3. RESULTS AND DISCUSSION

3.1. Structural properties

A detailed study of the crystalline structure of the Eu_2O_3 and $Eu_2Ti_2O_7$ before and after RTA treatment was realized by XRD measurements as shown in Figs. 1(a) and (b). A strong (622) peak and two weak (440) and (541) peaks are observed for the as-deposited Eu_2O_3 sample. In contrast, for the $Eu_2Ti_2O_7$ sample, two weak Eu_2O_3 (222) and $Eu_2Ti_2O_7$ (400) peaks were found in the 2θ diagram. At an annealing temperature of 700 °C, the strong Eu_2O_3 (400) reflection peak is observed in the XRD patterns, as shown in Fig. 1(a).

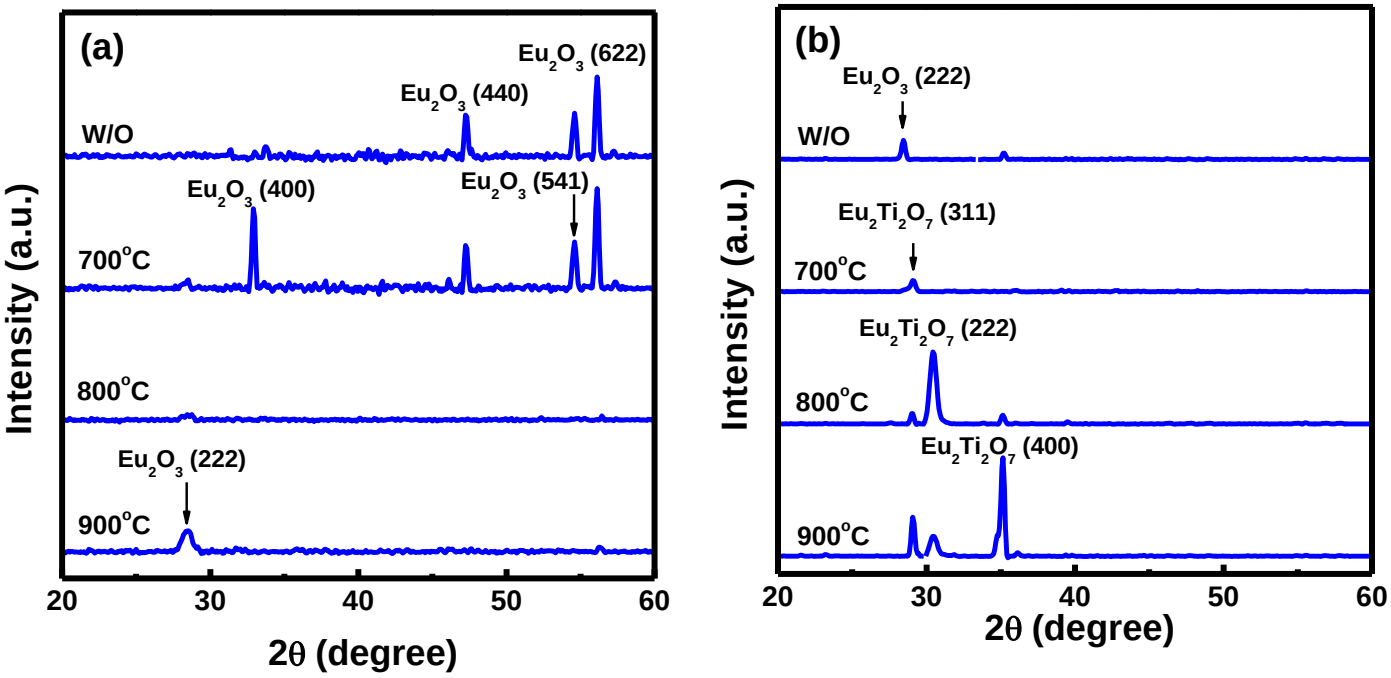

Figure 1. XRD patterns of (a) Eu_2O_3 and (b) $Eu_2Ti_2O_7$ films annealed at different temperatures.

Additionally, (440), (541) and (622) reflection peaks are observed but less intensity than for the (400) peak. A relatively small Eu_2O_3 (222) peak was found in the film annealed at 800 °C. At a higher annealing temperature of 900 °C, this (400) peak becomes slightly larger compared to 800 °C, suggesting a preferred (400) orientation of Eu_2O_3 film. However, the high temperature annealing will easily generate the formation of an amorphous SiO_2 and a nonstoichiometric silicate layer at the oxide/Si interface. In contrast, one strong (222) and two weak (311) and (400) peaks were found in the $Eu_2Ti_2O_7$ sample annealed at 800 °C, as shown in Fig. 1(b). The intensity of the $Eu_2Ti_2O_7$ (400) peak becomes stronger than that of the other peaks in the 900 °C spectrum, indicative of a preferential orientation of the crystallites with the (400) planes of $Eu_2Ti_2O_7$ parallel to the substrate.

Figure 2(a) shows the Eu 4d XPS spectra for the Eu_2O_3/Si interface after RTA treatment. The Eu $4d_{3/2}$ and $4d_{5/2}$ peaks of the reference Eu_2O_3 located at 141.1 and 135.6 eV [25], respectively. For the as-deposited films, the Eu 4d double peaks are shifted higher binding energy by about 0.8 eV as compared to the Eu_2O_3 reference position, indicating a poor $Eu(OH)_x$ structure due to the hydroxide formation after exposure to an air ambient [26].

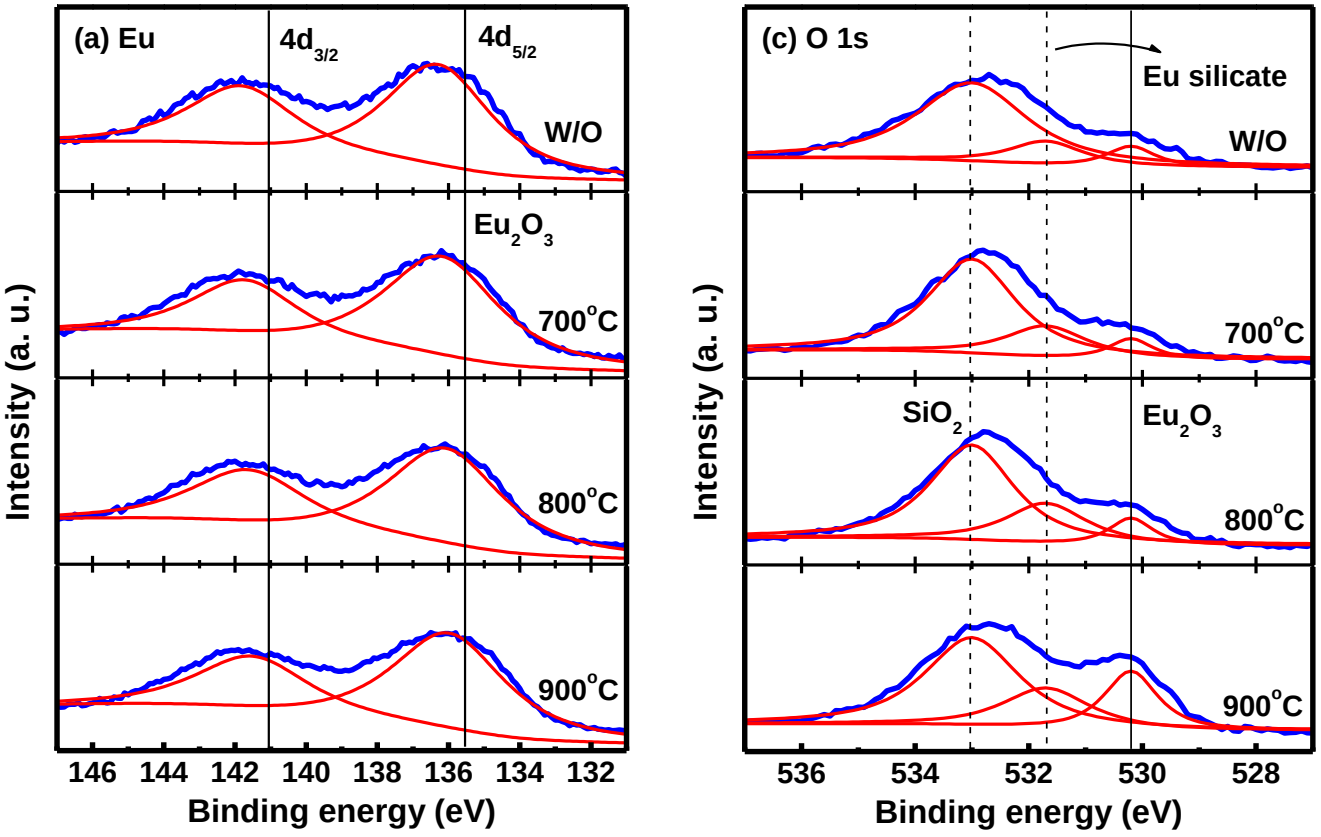

Figure 2. XPS spectra of (a) Eu 4d and (b) O 1s for Eu_2O_3 films after annealing at different temperatures.

The position of Eu 4d double peaks for the sample annealed at 700 and 800 °C shift to a lower binding energy relative to the $Eu(OH)_x$ position, suggesting a lesser amount of Eu reacting with OH leading to a thinner $Eu(OH)_x$. The chemical shift of the Eu 4d doublet peaks moved toward lower binding energy for the film annealed 900 °C ($4d_{3/2}$ and $4d_{5/2}$ peaks at 141.6 eV and 136.1 eV, respectively) as compared to the sample annealed 800 °C. This shift is due to the high Eu-contented metal oxide film. The O 1s spectra for the Eu_2O_3 films after RTA at different temperatures are shown in Fig. 2(b) with their appropriate peak curve-fitting lines corresponding to chemical states. Each fitting peak followed the general shape of the Lorentzian-Gaussian function. The low energy state at 530.2 eV is assigned to O in Eu_2O_3 [25]. The intermediate energy state at 531.7 eV is attributed to

interfacial O atoms in nonstoichiometric Eu-silicate ($EuSi_xO_y$). The high energy state at 533 eV is assigned to O in SiO_2 [27]. The intermediate energy feature at 531.7 eV is distinctly different from both O in SiO_2 and O in Eu_2O_3. The as-deposited sample appears to be composed of Eu_2O_3, Eu-silicate, and SiO_2. The intensity of the O 1s peak corresponding to Eu_2O_3 was rather constant up to 800 °C, but suddenly increased at 900 °C. Furthermore, the intensity of the O 1s peak corresponding to silicate gradually increases with increasing the RTA temperature, while the O 1s peak intensity corresponding to SiO_2 was rather constant accordingly. This result suggests that the high-temperature annealing increases the formation of an Eu silicate layer and amorphous silica at the Eu_2O_3/Si interface.

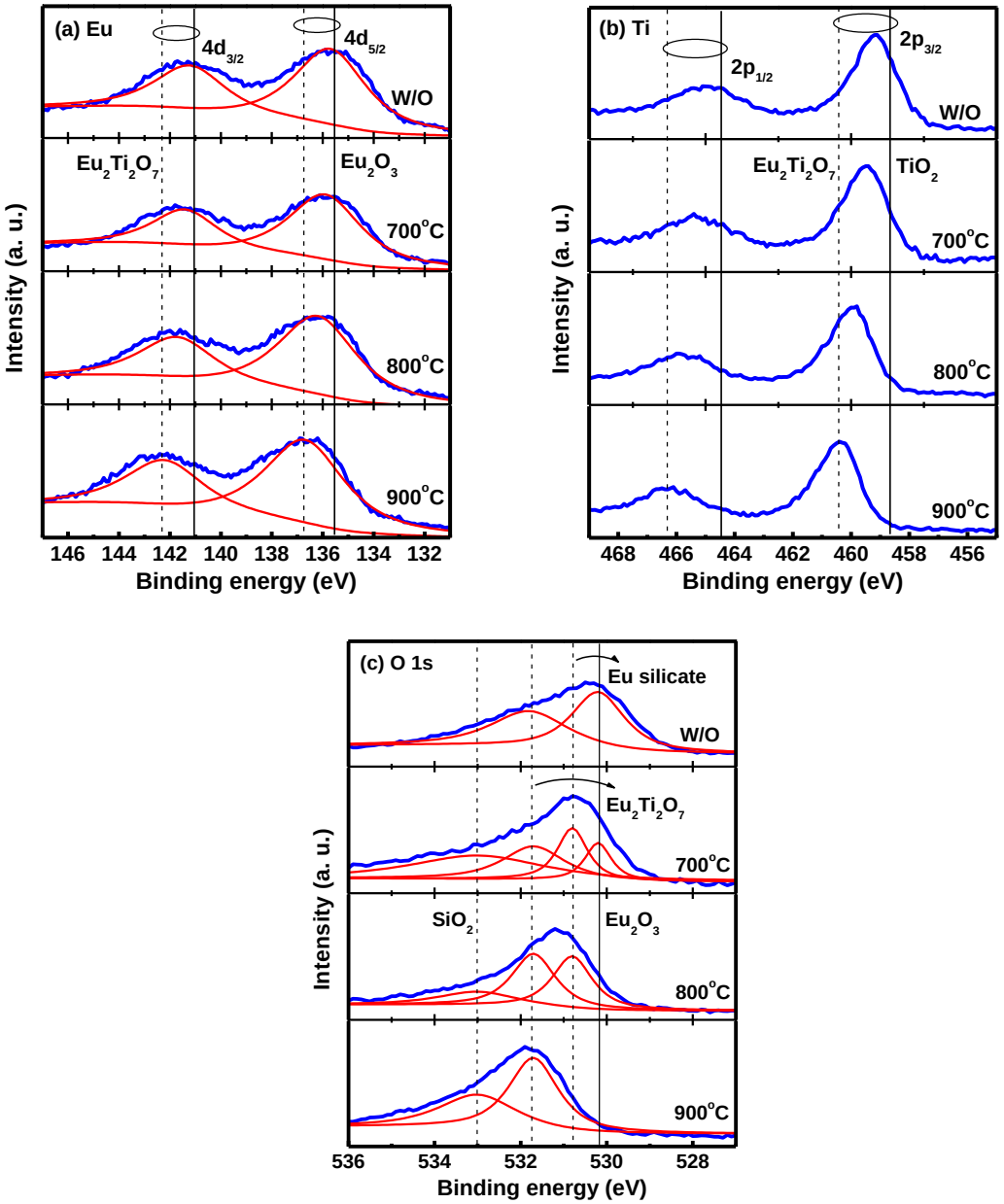

Figure 3. XPS spectra of (a) Eu 4d, (b) Ti 2p, and (c) O 1s for $Eu_2Ti_2O_7$ films after annealing at different temperatures.

Figure 3 shows the Eu 4d, Ti 2p, and O 1s core level XPS spectra for the $Eu_2Ti_2O_7$ film annealed at different temperatures. For the sample without RTA treatment, the Eu $4d_{3/2}$ and $4d_{5/2}$ peaks at 141.3 and 135.8 eV, respectively, suggest a poor $Eu_2Ti_2O_7$ structure. It is found that the shift of the Eu 4d peak to a higher binding energy increases upon increasing the RTA temperature. This can be explained by the formation of a better $Eu_2Ti_2O_7$ structure during high-temperature annealing. For annealing performed at 900 °C, the chemical shift of the Eu 4d core level moved toward higher binding energy for the case of the $Eu_2Ti_2O_7$ film ($4d_{3/2}$ and $4d_{5/2}$ peaks at 142.3 and 136.8 eV, respectively) as compared with the Eu_2O_3 film. The chemical shift to higher binding energy for Eu 4d peak indicates the difference between the Eu-O-Ti bonding in Eu_2O_3 and that in $Eu_2Ti_2O_7$. The peaks for the Ti $2p_{1/2}$ and $2p_{3/2}$ energy levels appeared at 464.7 and 459.1 eV, respectively, for the as-deposited $Eu_2Ti_2O_7$ film [Fig. 3(b)], indicating a poor TiO_2 structure incorporating Ti in the form of TiO_2 or TiOH, which probably formed in the surface region of the sample during its exposure to air [19]. For the film annealed at 900 °C, the Ti 2p doublet (Ti $2p_{1/2}$ and Ti $2p_{3/2}$ at 466 and 460.4 eV, respectively) is shifted to higher binding energy compared to the TiO_2 reference position (Ti $2p_{1/2}$ and Ti $2p_{3/2}$ at 464.3 and 458.7 eV, respectively) [19]. This shift was attributed to Ti in $Eu_2Ti_2O_7$ compound. Figure 3(c) displays the O 1s spectra with appropriate curve-fitting of peaks for the $Eu_2Ti_2O_7$ films after RTA treatment. In the four sets of spectra, the O 1s peaks at 533, 531.7, 530.8, and 530.2 eV represent the Si–O, Eu–O–Ti, Eu–O–Si, and Eu–O bonds [25], respectively. The as-deposited film exhibited one strong Eu_2O_3 and one weak $Eu_2Ti_2O_7$ peaks, suggesting a poorly crystalline structure. The O 1s peak intensity corresponding to Eu_2O_3 decreased upon increasing the RTA temperature, whereas the O 1s peak intensity corresponding to $Eu_2Ti_2O_7$ increased accordingly. This phenomenon is consistent with the reaction of O and Eu atoms with Ti atoms, forming a well-crystallized $Eu_2Ti_2O_7$ film. The O 1s peak corresponding to the Eu silicate components of the film annealed at 800 °C had higher intensity compared to 700 °C, suggesting that Eu atoms diffused from the high-k film to form a thicker Eu silicate layer at the $Eu_2Ti_2O_7$ and Si interface. On the other hand, the O 1s peak corresponding to the SiO_2 component of the film annealed at 900 °C had higher intensity compared to the film annealed 800 °C, possibly because oxygen atoms diffused from the high-k film to the oxide–Si interface, causing the formation of a thicker SiO_2 layer.

The surface roughness of the Eu_2O_3 and $Eu_2Ti_2O_7$ sensing films after PDA at various temperatures is shown in Figs. 4(a) and (b). The as-deposited Eu_2O_3 exhibited a larger surface roughness than the annealed film. The enhancement in surface roughness is possibly due to the moisture absorption of Eu_2O_3 resulting in the nonuniform volume expansion of the film [28]. It is found that the surface roughness of the Eu_2O_3 film decreases with increasing the RTA temperature. We believe that the Eu_2O_3 film is condensed during this annealing temperature as the density increase. For the annealed film, the $Eu_2Ti_2O_7$ sample shows a higher surface roughness compared with the Eu_2O_3 sample. This is attributed to that the Ti incorporating into the Eu_2O_3 film increased the growth of the grain size. Furthermore, the surface roughness of the $Eu_2Ti_2O_7$ film increases with increasing the RTA temperature. We suggest that this behavior is due to an increased self-diffusion of europium, titanium and oxygen during high-temperature annealing resulting in the enhancement of the clustering of grains, thus increasing the surface roughness of the $Eu_2Ti_2O_7$ film [14].

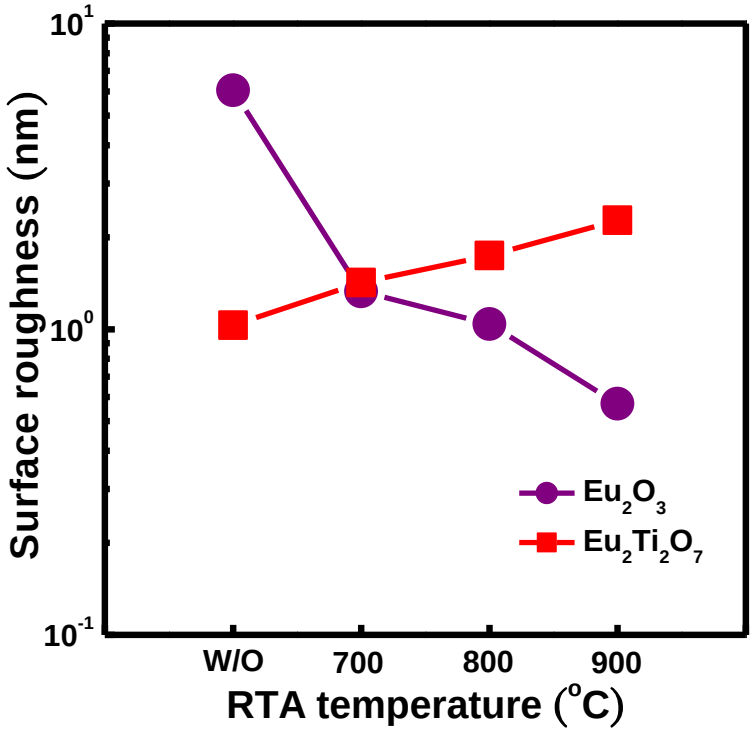

Figure 4. Surface roughness of Eu_2O_3 and $Eu_2Ti_2O_7$ films as a function of RTA temperature.

3.2. Sensing characterization

An output signal of EIS devices arises from the alteration of the gate potential due to changes of the membrane/electrolyte interfacial potential caused by changes in concentration of the hydrogen ions. According to the binding site theory of the membrane surface [29], the sensing characteristics of ISFET device are based on the electric double layer structure at the electrolyte/membrane interface. In this theory, effects of hydrogen ion exchange and physical and chemical adsorptions of anions, cations and neutral molecules are included water molecules (surface hydration). The flatband voltage (V_{FB}) of an EIS (or ISFET) device is the most important measurable parameter; it is defined the following equation [30]:

$$V_{FB} = E_{ref} - \psi_0 + \chi^{sol} - \frac{\Phi_{Si}}{q} - \frac{Q_{SS} + Q_{OX}}{C_{OX}} \quad \text{.....(1)}$$

where E_{ref} is the reference electrode potential relative to vacuum, ψ_0 is the pH-dependent surface potential, χ^{sol} is surface dipole potential of the solution, Φ_{Si} is the silicon workfunction, q is the electron charge, Q_{ss} is the density of interface states at the silicon surface, Q_{ox} is the fixed oxide charge, and C_{ox} is the capacitance of gate insulator layer. All terms in this equation are constant except for ψ_0, ψ_0 makes the EIS (or ISFET) device sensitive to the electrolyte pH, which depends on the dissociation of the insulator surface groups. The effect of the PDA temperature on the pH sensitivity of the Eu_2O_3 and $Eu_2Ti_2O_7$ sensing films can be understood by using the site-binding model to describe the ionic

absorption processes at the electrolyte/oxide interface. Figures 5(a) and (b) demonstrate the pH dependence of one group of *C–V* curves for the EIS structure prepared using a Eu_2O_3 and $Eu_2Ti_2O_7$ films annealed at 900 °C.

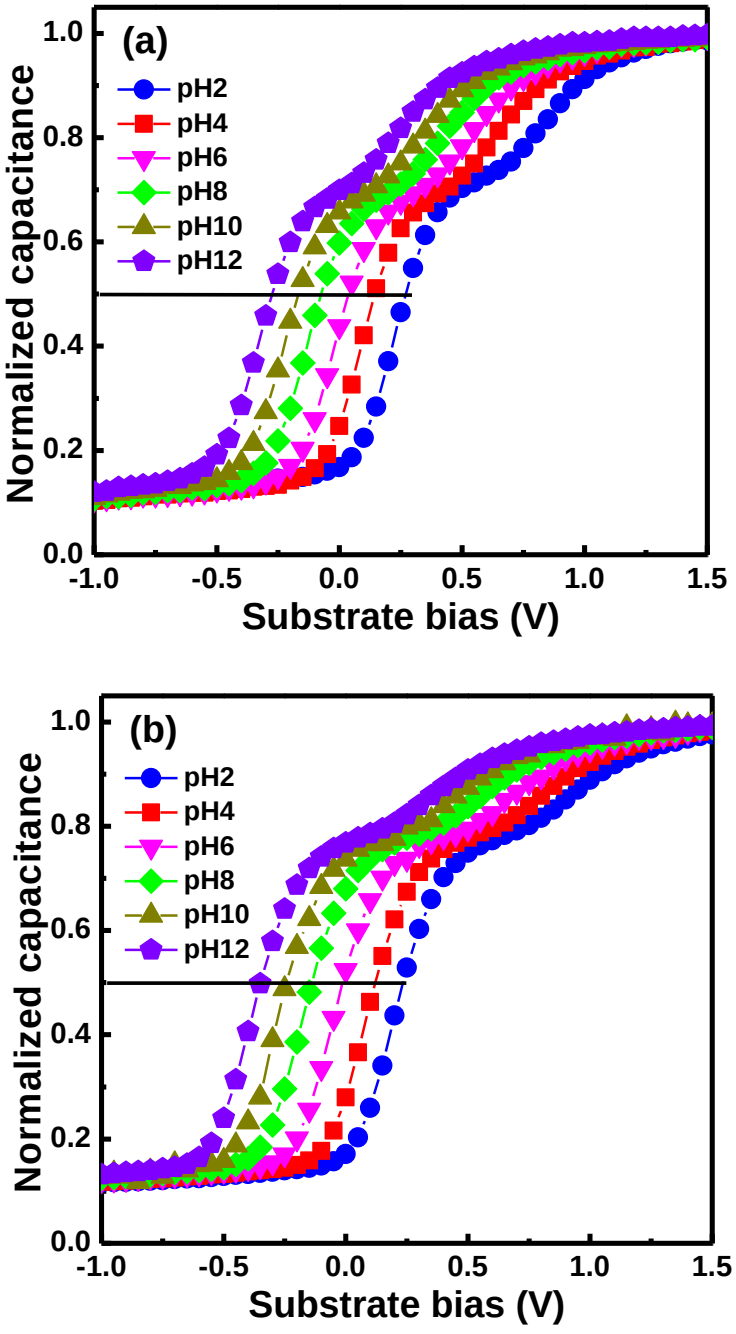

Figure 5. C-V curves response of (a) Eu_2O_3 and (b) $Eu_2Ti_2O_7$ sensing films annealed at 900 °C when inserted into solutions with pH values from 2 to 12. The inset shows the reference voltage of (a) Eu_2O_3 and (b) $Eu_2Ti_2O_7$ EIS devices annealed at 900 °C as a function of pH, measured at room temperature.

These normalized *C–V* curves were shifted as a result of H^+ ions modifying the surface potential through dipole formation on the sensing membrane. This EIS device has distorted *C–V* curves in the solutions from pH 2 to 12. This may be attributed to the presence of interface traps in the oxide. The insets (a) and (b) to Fig. 5 depict the pH dependence of the reference voltage (V_{REF}) of Eu_2O_3 and $Eu_2Ti_2O_7$ sensing membranes after RTA at 900 °C. During a cycle from pH 2 to 12, such a $Eu_2Ti_2O_7$ EIS device shows a high pH sensitivity of 59.03 mV/pH and good linearity of 99.9%.

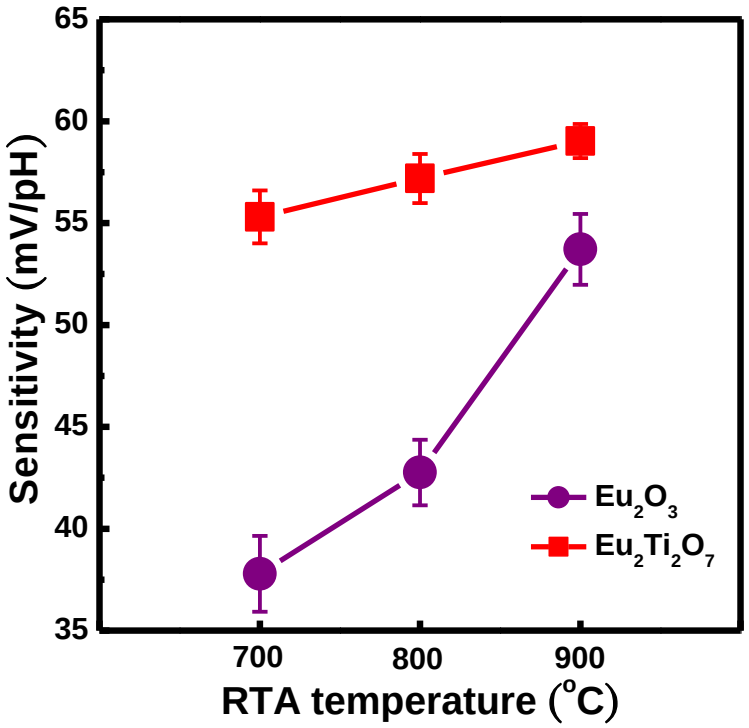

Figure 6. pH sensitivity as a function of RTA temperatures for EIS devices with Eu_2O_3 and $Eu_2Ti_2O_7$ sensing membranes.

To evaluate the sensing performance of the Eu_2O_3 and $Eu_2Ti_2O_7$ EIS devices after PDA at different temperatures, we recorded a set of *C–V* curves at the pH ranging from pH 2 to 12. The pH sensitivity of Eu_2O_3 and $Eu_2Ti_2O_7$ sensing membranes as a function of RTA temperatures is shown in Figs. 6(a) and (b). EIS devices using a $Eu_2Ti_2O_7$ film exhibit a higher pH sensitivity than that of the Eu_2O_3 film. This result could be attributed to the higher surface roughness of the $Eu_2Ti_2O_7$ sensing film as observed in the previous AFM analysis. With the higher surface roughness, the number of surface site will increase accordingly, which, therefore, contributes to a higher detection sensitivity as previously discussed in the site-binding model [12]. We find that the $Eu_2Ti_2O_7$ sensing membrane annealed at 900 °C has a higher pH sensitivity of 59.03 mV/pH as compared to other RTA temperatures. This is due to a larger surface roughness and the formation of a well-crystallized $Eu_2Ti_2O_7$ film during this RTA temperature, thus a high density of surface hydroxyl groups.

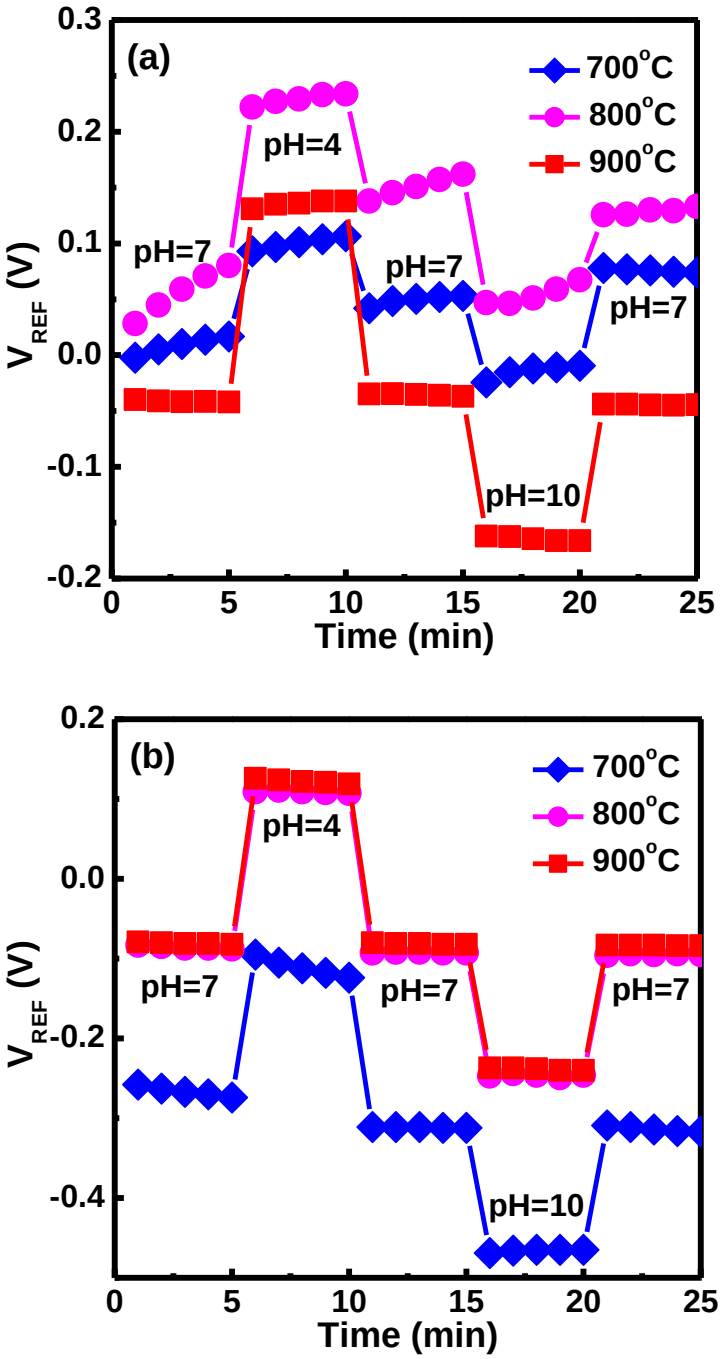

Figure 7. Hysteresis phenomenon of (a) Eu_2O_3 and (b) $Eu_2Ti_2O_7$ EIS devices annealed at various temperatures during the pH loop of 7→4→7→10→7.

Figures 7(a) and (b) depict the hysteresis phenomenon (reference voltage variation) of Eu_2O_3 and $Eu_2Ti_2O_7$ sensing films annealed at different temperatures during the pH loop of 7→4→7→10→7 over a period of 1500 s. The hysteresis characteristic can be due to the intrinsic defects of a dielectric film, causing the formation of porous structures. The interior sites of these porous defects could react with the ions existing in the tested solution and thus lead to a hysteresis response [7]. The hysteresis voltage here is defined as the reference voltage difference between the initial and terminal voltages

measured in the above cycle. The EIS device incorporating a $Eu_2Ti_2O_7$ sensing film exhibits a smaller hysteresis voltage than that of Eu_2O_3 film. This result is attributed to the fast response of such a $Eu_2Ti_2O_7$ EIS device due to a better $Eu_2Ti_2O_7$ structure, a lower defect chemistry, and a thinner interfacial layer. The $Eu_2Ti_2O_7$ EIS capacitor annealed at 900 °C had a smaller hysteresis voltage of 2.8 mV than other annealing temperatures.

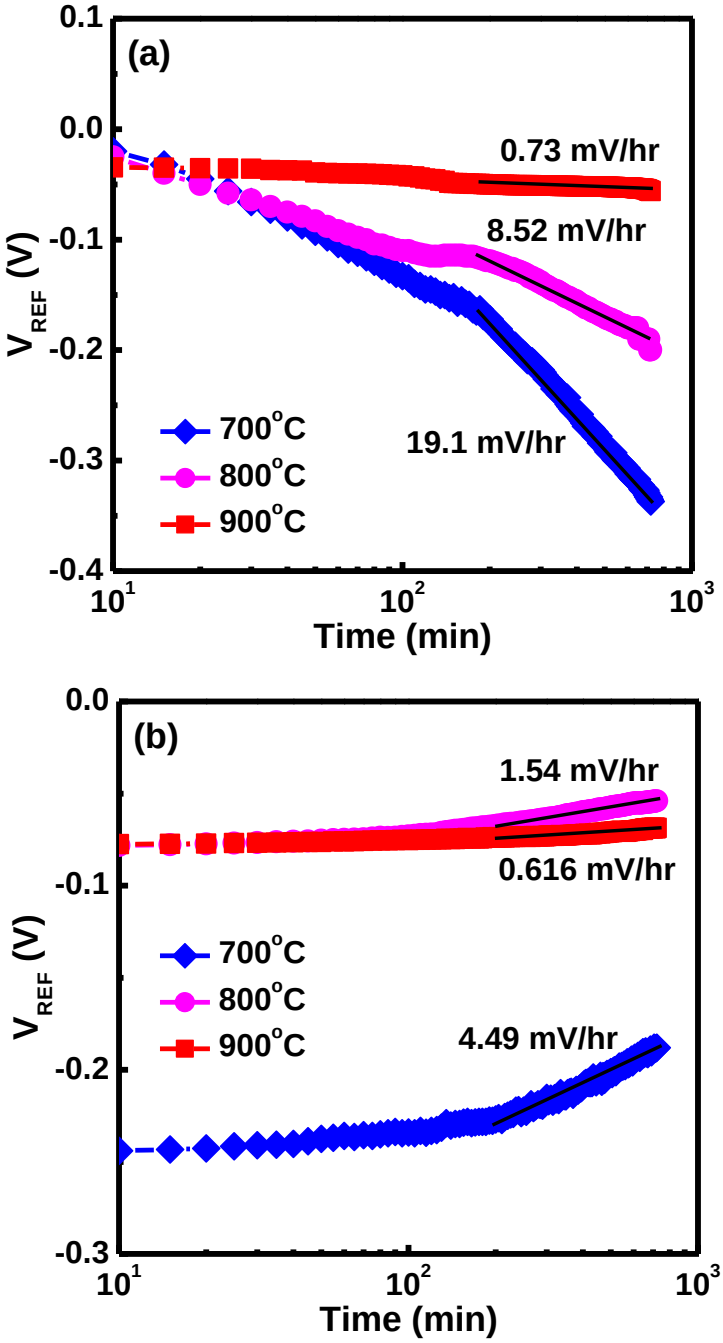

Figure 8. Drift characteristics as a function of times for (a) Eu_2O_3 and (b) $Eu_2Ti_2O_7$ EIS devices annealed at various temperatures, measured in the pH= 7 solution.

This is due to a low number of crystal defects. In contrast, the 700 °C-annealed sample shows a high hysteresis voltage variation, indicating a large density of crystal defects to create interior sites. These would be sites that can respond to changes of the chemical composition of the tested solution, causing large variations in the gate voltage.

Figures 8(a) and (b) show the drift characteristics of EIS devices using Eu_2O_3 and $Eu_2Ti_2O_7$ films annealed at various temperatures as a function of time, measured in the pH 7 solutions for 12 h. The drift rate of a pH-ISFET can be explained through the penetration of ions contained in the electrolyte into the sensing film [32]. The charged electrolyte ions can penetrate the hydrated layer of the sensing film and lead to the decrease in effective gate oxide thickness [6]. Therefore, the change of gate capacitance produces the non-ideal effects in the ISFETs. The total amount of penetrating ions and the duration of the penetration process depend on the ion mobility of the sensing film. The change in the reference voltage can be written as $\Delta V_{REF}=V_{REF}(t)-V_{REF}(0)$. The degradation slope of the reference voltage variation reflects the stability of an EIS device. For the film annealed at 900 °C, the $Eu_2Ti_2O_7$ sensing film exhibited a better stability of 0.616 mV/h compared to the Eu_2O_3 film. The drift effect was improved by the low mobility of ions due to the low density of crystal defects in the film. However, a higher drift rate of the Eu_2O_3 and $Eu_2Ti_2O_7$ films annealed at 700 °C was considered to be caused by a higher density of crystal defects producing the high mobility of ions.

Table 1. Comparison of sensing parameters for an EIS device fabricated with a Si_3N_4, Al_2O_3, Ta_2O_5, HfO_2, Yb_2O_3, $PrTiO_3$, Eu_2O_3, and $Eu_2Ti_2O_7$.

Sensing membrane	pH sensivity (mV/pH)	Hysteresis voltage (mV)	Drift rate (mV/h)
Si_3N_4	53-55	3	0.8
Al_2O_3	54-56	0.8	0.3
Ta_2O_5	55-58	< 1	0.2
HfO_2	58.3	1.7	0.6
Yb_2O_3	55.5	3.76	1.54
$PrTiO_3$	56.8	2.84	5.4
Eu_2O_3	53.71	3.1	0.73
$Eu_2Ti_2O_7$	59.03	2.8	0.616

The measured as well as extracted sensing parameters are summarized in Table 1, where the data from EIS devices incorporating a Si_3N_4 [33-34], Al_2O_3 [33-34], Ta_2O_5 [2], HfO_2 [9], Yb_2O_3 [12], and $PrTiO_3$ [35], are shown for comparison. Although a $Eu_2Ti_2O_7$ sensing membrane has a slightly higher hysteresis and larger drift than an Al_2O_3 sensing film, the nitrogen incorporated into the $Eu_2Ti_2O_7$ film can reduce the low-k silica layer at the oxide/Si interface and hence improve the sensing characteristics [13].

3.3. Creatinine $Eu_2Ti_2O_7$ EIS biosensor

We prepared an enzymatic $Eu_2Ti_2O_7$ EIS biosensor of our device, using creatinine deiminase as the biocomponent. Fig. 9(a) illustrates the hybrid configuration of our high-κ $Eu_2Ti_2O_7$ EIS (after RTA

at 900 °C) biosensor, which measured the creatinine concentration by detecting the variation in pH caused by the generation of HO^- ions upon the dissociation of creatinine.

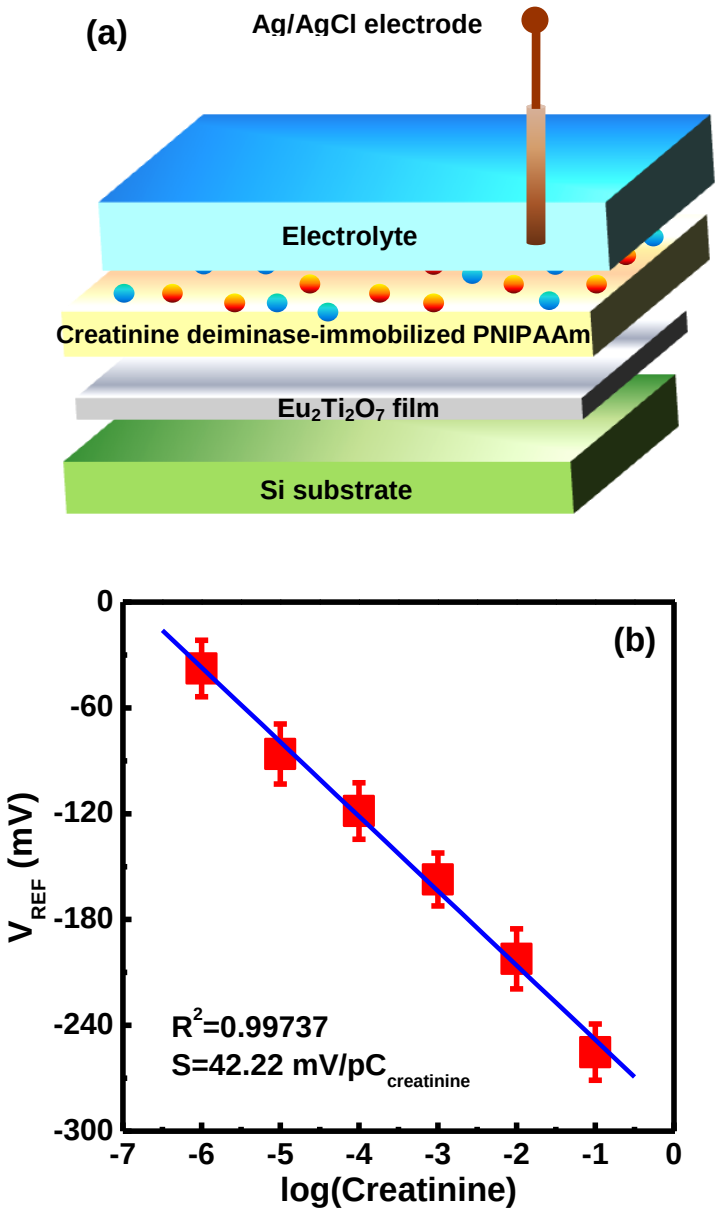

Figure 9. (a) Scheme of hybrid configuration of creatinine EIS biosensor and (b) the typical calibration curves of a $Eu_2Ti_2O_7$ EIS biosensor for creatinine.

The creatinine deiminase enzyme releases NH_3 from creatinine, forming NH_4^+ and HO^- ions. Compared with the carrier-binding method, the immobilization of enzyme molecules onto a transducer through gel entrapment method is commonly believed to be milder for enzyme molecules, and to be simpler for preparation [4]. Furthermore, in the real application of a biosensor, the repeated operations might cause contamination, which might in turn lead to the variation in several biochemical conditions (e.g. pH or enzyme activity) [21]. The inconsistency of such bio-recognition element could result in bias between run-to-run detection. To avoid this problem, a disposable bio-recognition element is

required to carry out each sensing task individually. Consequently, we proposed to use a disposable PNIPAAm as an encapsulating enzyme material. Making use of the phase tunable characteristics of this polymer, a bio-recognition element (creatinine deiminase-containing PNIPAAm film) can be easily loaded onto, and removed from the surface of a transducer. To demonstrate its feasibility for biosensing application, creatinine deiminase-containing PNIPAAm suspension was prepared and was loaded onto the $Eu_2Ti_2O_7$ membrane of EIS biosensor. The creatinine deiminase/PNIPAAm suspension loaded on the surface of a $Eu_2Ti_2O_7$ EIS sensor was heated at 37 °C and then this suspension became a creatinine deiminase/PNIPAAm gel. The EIS biosensor devices were immersed into the solutions with various creatinine concentrations to make *C-V* measurements. After *C-V* measurements, the creatinine deiminase/PNIPAAm gel was decreased its temperature below 32 °C and thus this gel was washed away by using R.O. water to remove completely it on the surface of such an EIS device. Fig. 9(b) presents the change in response voltage of the creatinine deiminase-immobilized $Eu_2Ti_2O_7$ EIS biosensor plotted with respect to the creatinine concentration. Based on the calibration curve, the sensitivity of this EIS biosensor is 42.22 mV/mM in the creatinine concentration range of 10^{-1}–10^{-6} M. The $Eu_2Ti_2O_7$ EIS device is a very promising biosensor for general clinical examination of blood creatinine.

4. CONCLUSION

In this paper, we investigated the structural and sensing properties of high-k Eu_2O_3 and $Eu_2Ti_2O_7$ sensing films deposited on a Si (100) substrate through reactive rf sputtering. We used XRD, XPS, and AFM analyses to confirm the presence of Eu_2O_3 and $Eu_2Ti_2O_7$ structures in the EIS devices. The EIS device incorporating the $Eu_2Ti_2O_7$ film and that had been annealed at 900 °C exhibited a higher sensitivity (59.03 mV/pH), a smaller hysteresis voltage (2.8 mV), and a lower drift rate (0.616 mV/h), relative to those of the systems that had been subjected to other annealing conditions. This result is attributed to the well-crystallized $Eu_2Ti_2O_7$ structure, suppression of the formation of an interfacial layer at the oxide/Si interface, and its higher surface roughness. To avoid the cross contamination and the reluctant detection bias problems during the repeated operations of biosensing, a simple concept of using a disposable enzyme/polymer film for an EIS biosensor was tested. In this work, we proposed the phase tunable properties of a thermosensitive PNIPAAm material to encapsulate creatinine deiminase, making easy the loading and removal of a creatinine deiminase/PNIPAAm film on a transducer. This becomes a more practical and efficient way to prepare a fresh bio-recognition element for each run of biosensing, which helps to solve the problems associated with the lifetime and the stability of enzyme molecules. We also prepared an $Eu_2Ti_2O_7$ EIS biosensor that could detect creatinine with reasonable sensitivity (42.22 mV/p$C_{creatinine}$) in solutions containing creatinine at concentrations in the range 10^{-1}–10^{-6} M; this sensitivity is adequate for general clinical examination of blood creatinine. EIS devices incorporating $Eu_2Ti_2O_7$ sensing membranes appear to be very promising systems for use in biomedical engineering applications.

ACKNOWLEDGMENT
This work was supported by the National Science Council, Taiwan, Republic of China, under contract no. NSC-98-2111-E-182-056-MY3 and NSC-99-2112-M-182-001-MY2.

References

1. P. Bergveld, *Sens. Actuators B*, 88 (2003) 1.
2. A.Poghossian and M. J. Poghossian, *Electroanalysis*, 16 (2004) 1863.
3. S. Caras and J. Janata, *Anal. Chem.*, 52 (1980) 1935.
4. B. R. Eggins, *Chemical Sensors and Biosensors*, John Wiley & Sons, New York (2002).
5. P. A. Estrela, G. Stewart, F. Yan, and P. Migliorato, *Electrochim. Acta*, 50 (2005) 4995.
6. L. Bousse, S. Mostarshed, B. van der Schoot, and N. F. de Rooij, *Sens. Actuators B*, 17, 157 (1994) .
7. L. Bousse, H. H. van der Vlekkert, and N. F. de Rooij, *Sen. Actuators B*, 2 (1990) 103.
8. S. Yoshida, N. Hara, and K. J. Sugimoto, *J. Electrochem. Soc.*, 151 (2004) H53.
9. C. M. Yang, C. S. Lai, T. F. Lu, T. C. Wang, and D. G. Pijanowska, *J. Electrochem. Soc.*, 155 (2008) J326.
10. L. B. Chang, H. H. Ko, Y. L. Lee, C. S. Lai, and C. Y. Wang, *J. Electrochem. Soc.*, 153 (2006) G330.
11. T. M. Pan, J. C. Lin, M. H. Wu, and C. S. Liao, *Sen. Actuators B*, 133 (2009) 619.
12. T. M. Pan, C. H. Cheng, and C. D. Lee, *J. Electrochem. Soc.*, 156 (2009) J108.
13. G. D. Wilk, R. M. Wallace, and J. M. Anthony, *J. Appl. Phys.*, 89 (2001) 5243.
14. M. Fanciulli and G. Scarel, (Eds.), *Rare Earth Oxide Thin Film: Growth, Characterization, and Applications*, Springer, Berlin (2007).
15. O. Engstrom, B. Raeissi, S. Hall, O. Buiu, M. C. Lemme, H. D. B. Gottlob, P. K. Hurley, and K. Cherkaoui, *Solid State Electron.*, 51 (2007) 622.
16. J. Paivasaari, M. Putkonen, and L. Niinisto, *Thin Solid Films*, 472 (2005) 275.
17. R. B. van Dover, *Appl. Phys. Lett.*, 74 (1999) 3041.
18. T. Schroeder, G. Lupina, J. Dabrowski, A. Mane, Ch. Wenger, G. Lippert, and H. J. Mussig, *Appl. Phys. Lett.*, 87 (2005) 022902.
19. S. Jeon and H. Hwang, *Appl. Phys. Lett.*, 81, 4856 (2002).
20. D. G. Pijanowska, A. Baraniecka, R. Wiater, G. Ginalska, J. Lobarzewski, and W. Torbicz, *Sens. Actuators B*, 78 (2001) 263.
21. W. Tischer and F. Wedekind, *Top. Curr. Chem.*, 200 (1999) 95.
22. K. Wan, J. M. Chovelon, and N. Jaffrezic-Renault, *Talanta*, 52 (2000) 663.
23. Y. Hirokawa and Y. J. Tanaka, *J. Chem. Phys.*, 81 (1984) 6379.
24. X. Yin, A. S. Hoffman, and P. S. Stayton, *Biomacromolecules*, 7, 1381 (2006).
25. Y. Uwamino, Y. Ishizuka, and H. Yamatera, *J. Electron Spectrosc. Relat. Phenom.*, 34 (1984) 67.
26. Y. Zhao, K. Kita, K. Kyuno, and A. Toriumi, *Appl. Phys. Lett.*, 89 (2006) 252905.
27. J. F. Moulder, W. F. Stickle, P. E. Sobol, and K. D. Bomben, *Handbook of X-Ray Photoelectron Spectroscopy: A Reference Book of Standard Spectra for Identification and Interpretation of XPS Data*, Physical Electronics, Eden Prairie, MN (1995).
28. Y. Zhao, M. Toyama, K. Kita, K. Kyuno, and A. Toriumi, *Appl. Phys. Lett.*, 88 (2006) 072904.
29. C. D. Fung, P. W. Cheung, and W. H. Ko, *IEEE Trans. Electron Devices*, 33 (1986) 8.
30. P. Bergveld and A. Sibbald, *Comprehensive analytical chemistry: v.23: Analytical and Biomedical Applications of Ion-Selective Field-Effect Transistors*, Elsevier Science Publishing Company Inc, New York (1988).
31. L. Bousse, N. F. de Rooij, and P. Bergveld, *IEEE Trans. Electron Devices*, 30 (1983) 1263.
32. C. C. Wen, T. C. Chen, and J. N. Zemel, *IEEE Trans. Electron Devices*, 26 (1979) 1845.

33. Y. Miao, J. Guan, and J. Chen, *Biotechnol. Adv.*, 21 (2003) 527.
34. T. Matsuo, M. Esashi, and H. Abe, *IEEE Trans. Electron Devices*, 26 (1979) 1856.
35. T. M. Pan and K. M. Liao, *Sen. Actuators B*, 133 (2008) 97.